Electronic Supplementary Material (ESI) for Journal of Materials Chemistry B.

Supporting Information:

Silk Fibroin-based Hemostatic Powders with Instant and Robust Adhesion Performance for Sutureless Sealing of Gastrointestinal Defects

Aizhen Geng,[a] Yuting Luo,[b] Min Zheng,[a] Jie Zheng,[a] Rui Zhu[a] and Shumeng Bai*[a]

[a] College of Biological Science and Engineering, Fuzhou University, Fuzhou, Fujian 350108, China.

[b] College of Chemistry, Fuzhou University, Fuzhou, Fujian 350108, China.

* Corresponding author:

Email: shumengbai@fzu.edu.cn.

Supporting Figures

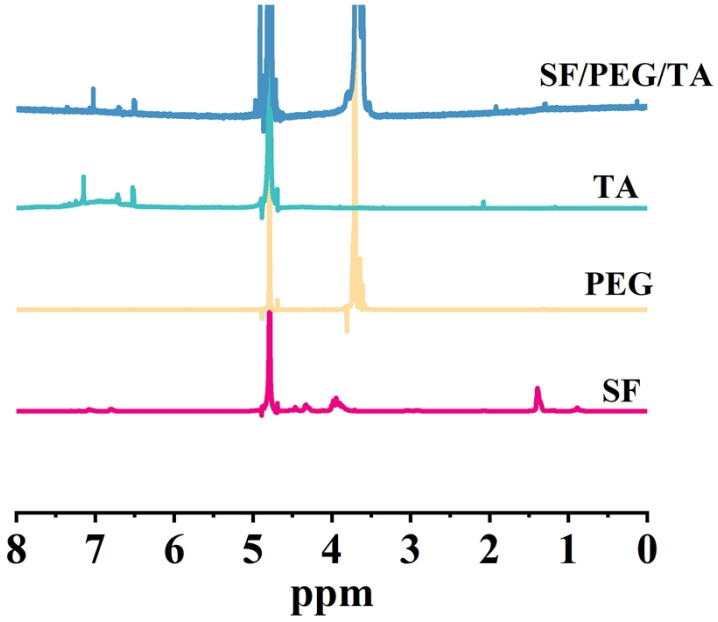

Figure S1. ^{1}H-NMR spectra of the SF/PEG/TA powder and its starting components.

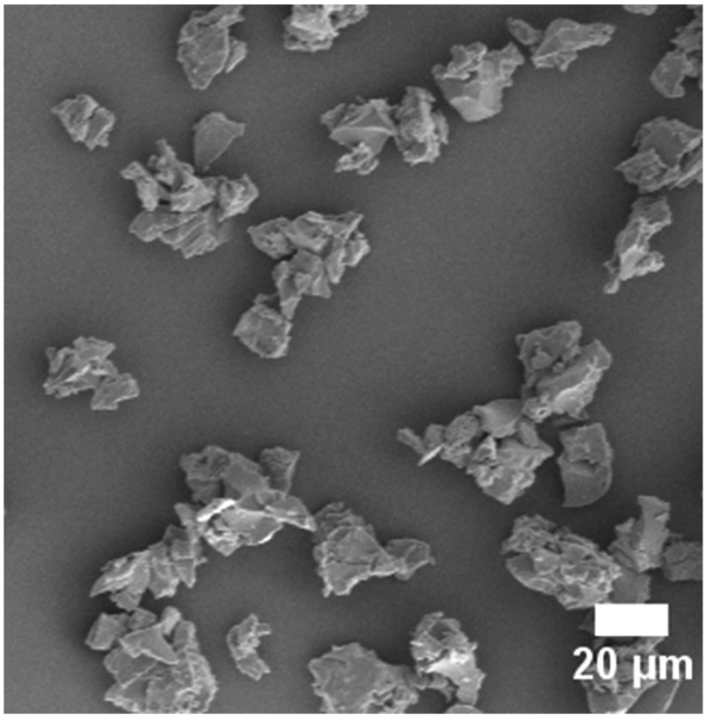

Figure S2. The average size of the SF/PEG/TA powder.

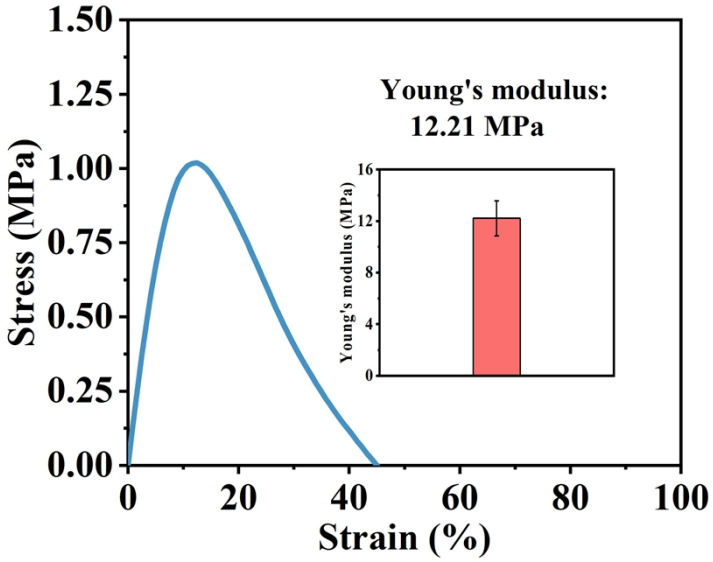

Figure S3. Representative tensile strain-stress curve of the SF/PEG/TA powder-derived hydrogel.

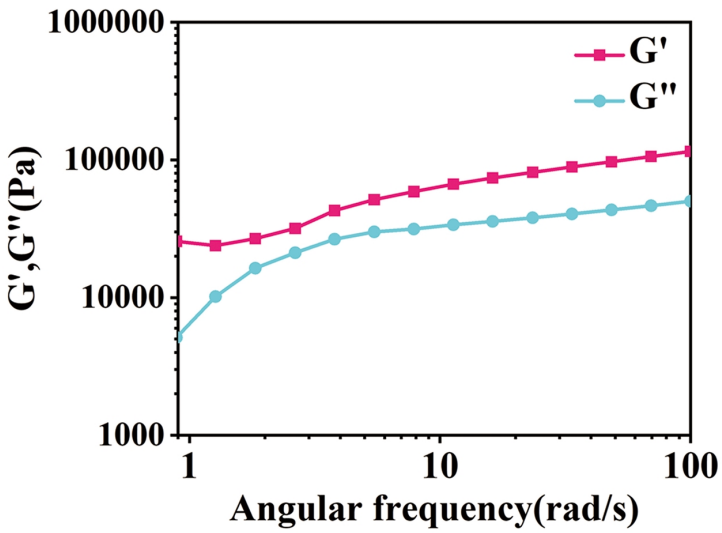

Figure S4. The frequency-dependent oscillatory rheology of SF/PEG/TA powder-derived hydrogel, validating the stable gel-like behavior across the whole range of frequencies.

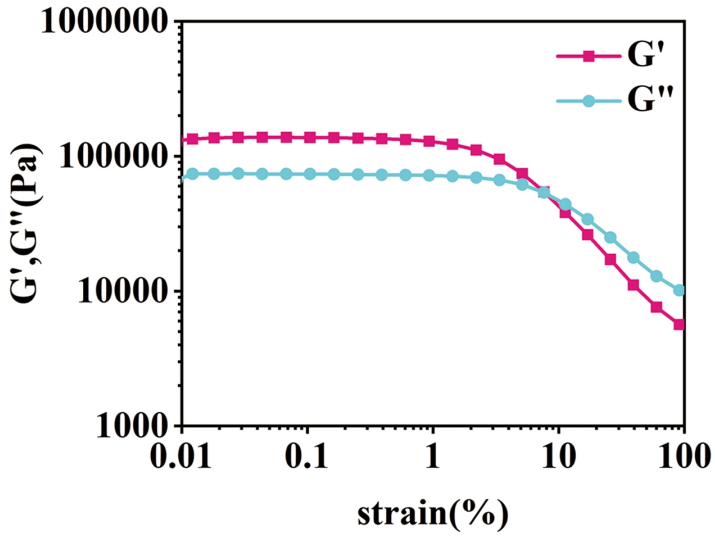

Figure S5. Strain-dependent oscillatory rheology of SF/PEG/TA powder-derived hydrogel at a constant angular frequency (10 rad s^{-1}).

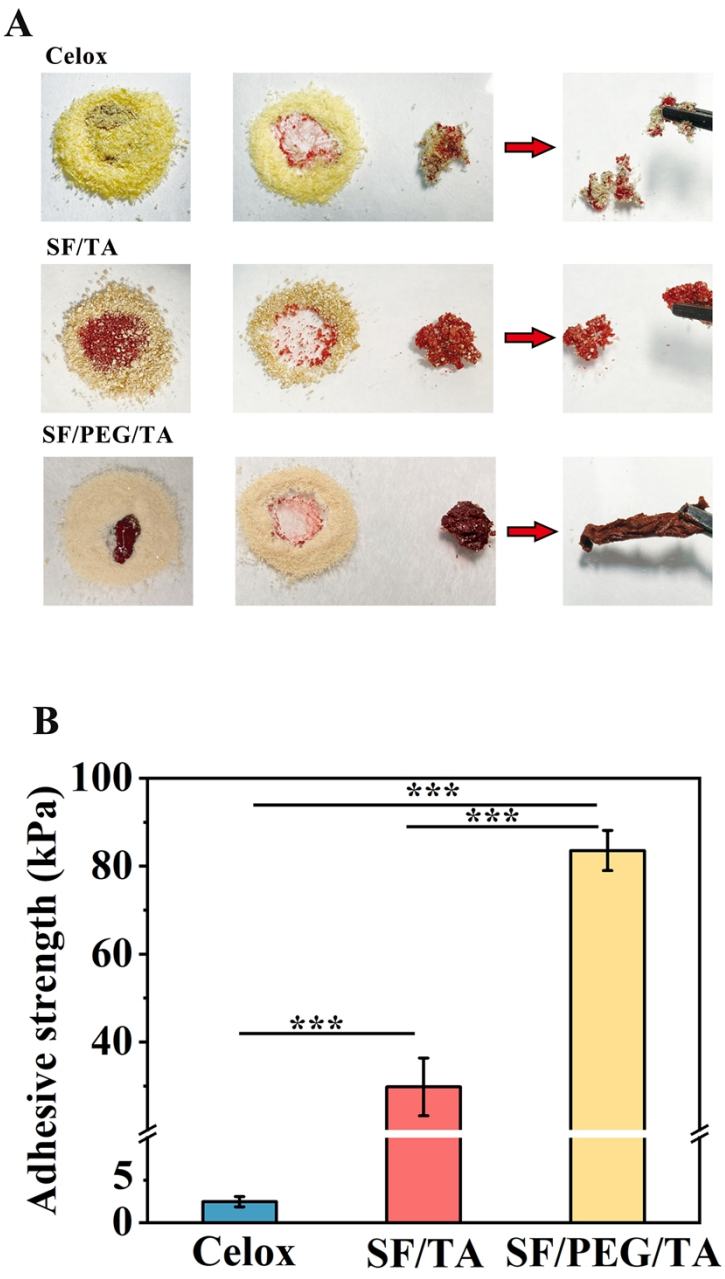

Figure S6. (A) The wet adhesion performance of SF/PEG/TA powder driven by self-gelling upon contact with the blood. (B) Corresponding adhesion strength of SF/PEG/TA powder on the plastic substrate via a lap shear adhesion test.

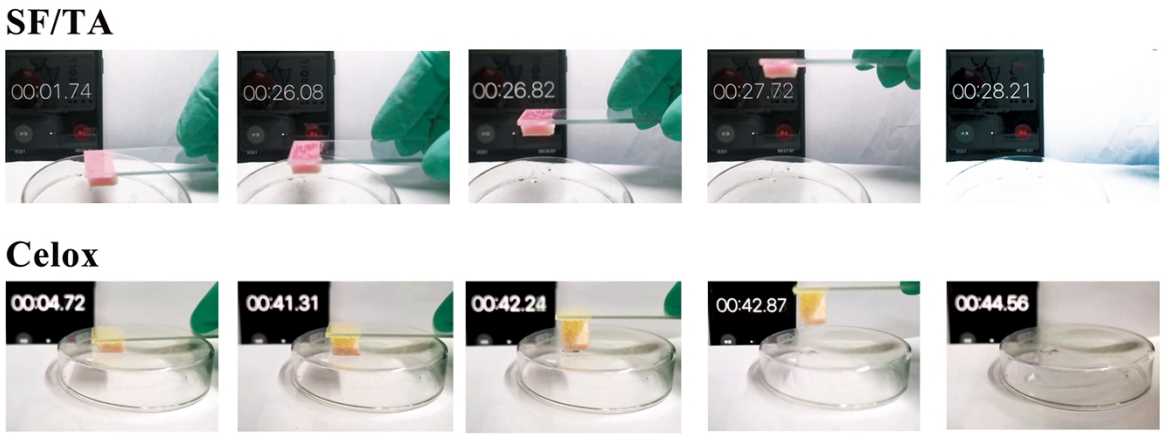

Figure S7. Photos of SF/TA or Celox powder fixed on a glass plate to adhere to wet porcine skin.

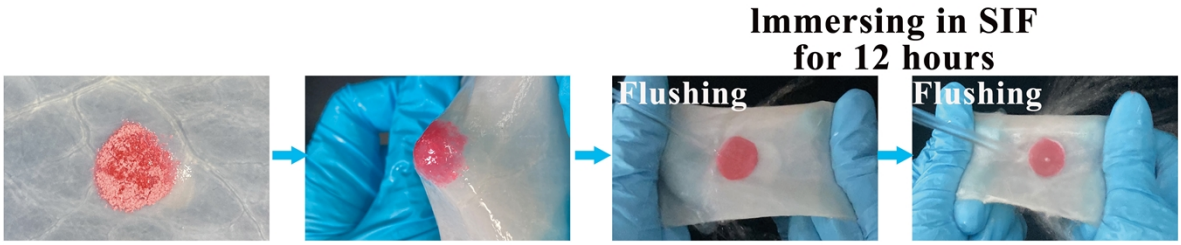

Figure S8. Adhesion images of Rhodamine B-stained SF/PEG/TA powder on wet porcine intestine.

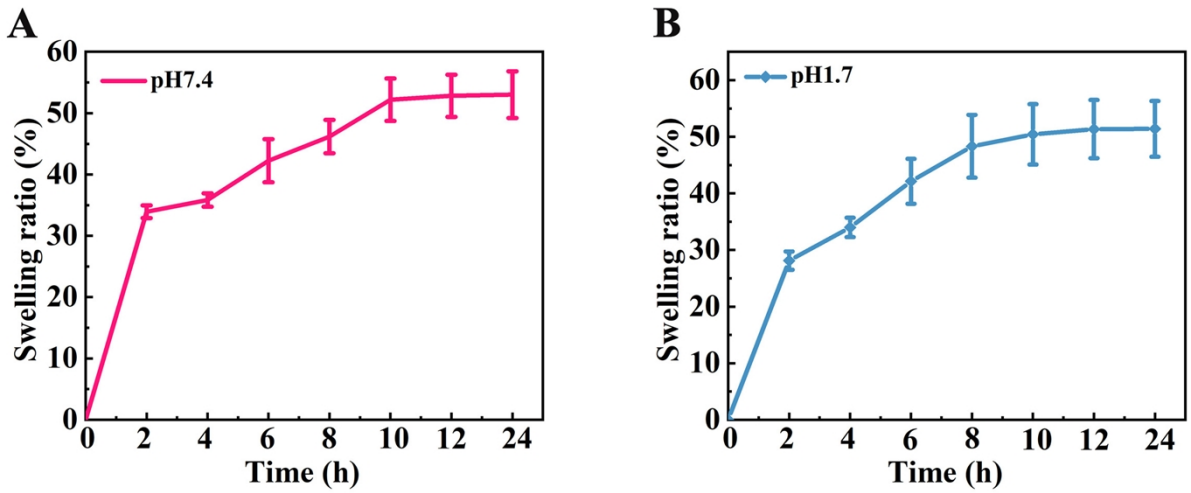

Figure S9. The in vitro swelling behavior of the SF/PEG/TA powder-derived hydrogel in phosphate buffered saline (PBS, pH 7.4 or 1.7) at 37 °C for 24 hours.

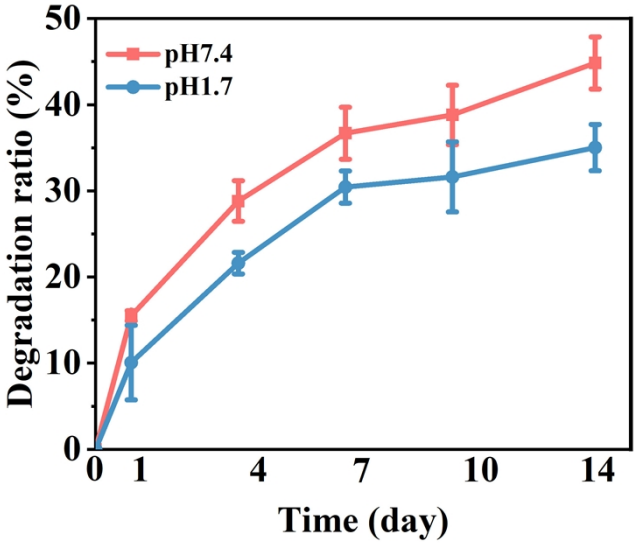

Figure S10. The in vitro degradation of the SF/PEG/TA powder-derived hydrogel in aqueous solution of 1 U mL^{-1} protease XIV (PBS, pH 7.4 or 1.7).

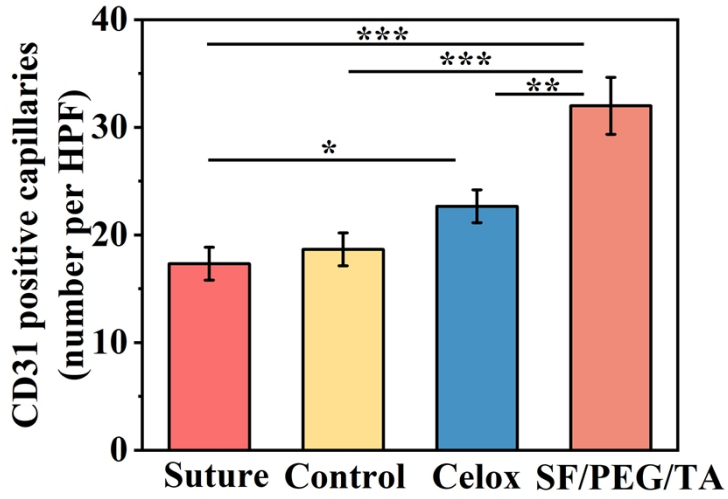

Figure S11. Quantitative analysis of CD31-positive capillaries for different groups in a rat skin incision model.

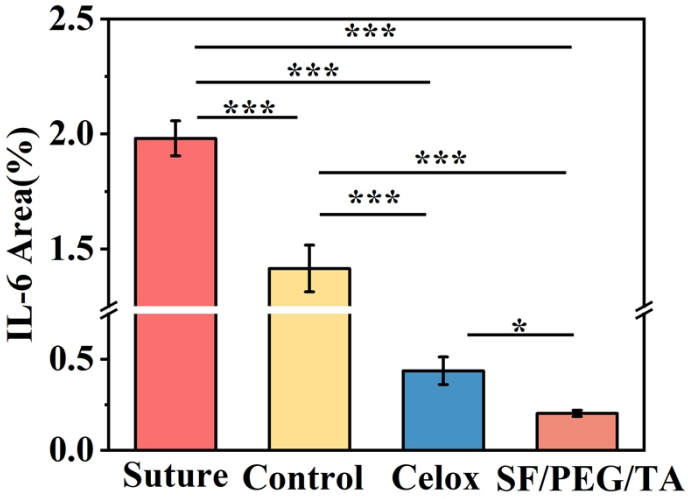

Figure S12. Quantitative analysis of the relative fluorescent intensity of IL-6 for different groups in a rat skin incision model.

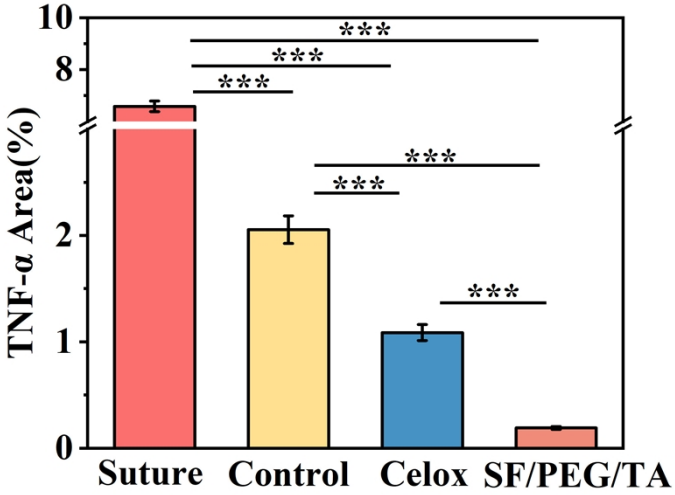

Figure S13. Quantitative analysis of the relative fluorescent intensity of TNF-α for different groups in a rat skin incision model.

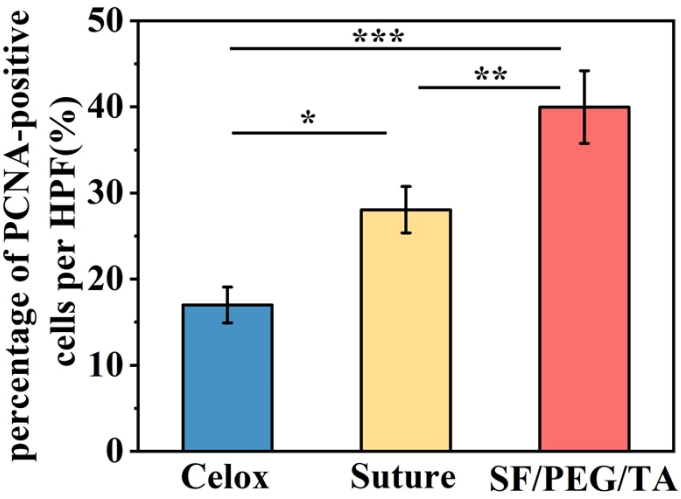

Figure S14. Quantitative analysis of PCNA-positive cells for different groups in a rat gastrointestinal perforation model.

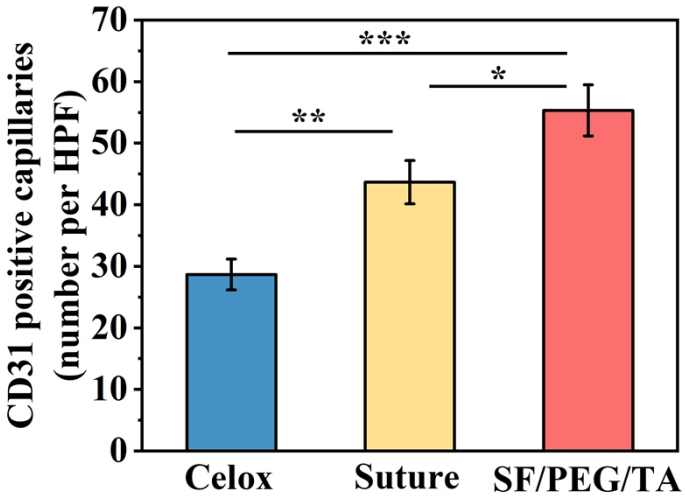

Figure S15. Quantitative analysis of CD31-positive capillaries for different groups in a rat gastrointestinal perforation model.